Synthesis and characterization of α-Fe_2O_3 Nanoparticles and α-Fe_2O_3 /TiO_2 Nanocomposite and application them in a solar cell

Ghanem Abdulnabi Kadhim 1 , a, Amer Musa Juda1, b

[1]Chemistry Department, Faculty of Science, Kufa University, Najaf, Iraq.

a) Corresponding author: ghanemn.alkreete @student .uokufa.edu.iq

b) ameralshamari235@gmail.com

Abstract:

Nanostructures of metal oxides of TiO_2 and α-Fe_2O_3 were prepared through the hydrothermal method. Also α-Fe_2O_3/TiO_2 nanocomposites are that prepared by the hydrothermal technique using and α-Fe_2O_3/TiO_2 nanocomposites are mixed in an equal ratio. The properties of the prepared compounds wear investigated through Transmission electron microscopy (TEM), X-rays diffraction, and field emission scanning electron microscopy (FE-SEM) The images of FE-SEM have confirmed that the prepared TiO_2 and α-Fe_2O_3NPs are structured as (Nanoparticles, plate-structure) respectively, and α-Fe_2O_3/TiO_2 nanocomposites are mixed in the equal ratio is structured as (spherical like structure). The results of the X-rays diffraction indicated the presence of TiO_2 and α-Fe_2O_3 a(Tetragonal, and Hexagonal) respectively. with the average crystallite sizes(8.65,7.10 , and 9.87) nm, forTiO_2 , α-Fe_2O_3 and α-Fe_2O_3/TiO_2 respectively .The optical properties of prepared compounds was studied through UV-Vis Spectroscopy. The optical band gap is (3.0, 1.6 and 2.7) ev for TiO_2, α-Fe_2O_3 NPs and α-Fe_2O_3/ TiO_2 nanocomposites. Dye-sensitized solar cells (DSSCs) fabricated depending on TiO_2, α-Fe_2O_3 NPs and α-Fe_2O_3/TiO_2/ nanocomposites are casted onto Fluorine-doped Tin Oxide (FTO) substrates front electrode. while the back electrode is a carbon/FTO-glass substrate. Green leek dye and red pomegranate dye were used as two natural dyes, while iodine /iodide KI/ I_2 was used as the electrolyte solution.. The solar cells efficiency rates (0.65, 1.38 and 0.96) for TiO_2, α-Fe_2O_3Nps and α-Fe_2O_3/TiO_2/ nanocomposites/red pomegranate dye respectively. and The solar cells' efficiency rates are (0.69, 1.93 and 1.29) for TiO_2, and α-Fe_2O_3/TiO_2/ nanocomposites/ green leek dye respectively.

Keywords: Nanocomposite, Hydrothermal, DSSCs.

الخلاصة:

تم تحضير أكاسيد المعادن ذات الهياكل النانوية لـ TiO_2 و α-Fe_2O_3 من خلال الطريقة الحرارية المائية. تم أيضًا تحضير المتراكب النانوي TiO_2/ α-Fe_2O_3 باستخدام التقنية الحرارية المائية باستخدام نسبة متساوية 1: 1 تم فحص خصائص المركبات المحضرة من خلال الفحص المجهري الإلكتروني الماسح (FE-SEM) وحيود الأشعة السينية (X-rays). أكدت صور FE-SEM أن TiO_2 و α-$Fe2O_3$ منظمة على شكل (نانوية ،على شكل الواح) . بينما شكل المتراكب و TiO2 / Fe2O3 بنسبة (1:1) منظمة على شكل (هيكل يشبه الكروي) على التوالي. أشارت نتائج حيود الأشعة السينية إلى وجود كل من TiO_2و α- Fe_2O_3 على شكل (رباعي الزوايا ، سداسي) على التوالي مع متوسط أحجام البلورات (9.87.7.10,8.65) نانومتر لـ TiO_2، α-Fe_2O_3 و TiO_2/ α-Fe_2O_3 على التوالي. درست الخصائص البصرية للمركبات المحضرة باستخدام مطافية Vis-UV. ، كانت طاقة الفجوة(2.7,1.6,3.0)الكترون فولت للمركبات TiO_2,α-Fe_2O_3 و TiO_2/ α-Fe_2O_3.

تم تصنيع الخلايا الشمسية الصبغية (DSSCs) على أساس المركبات النانوية TiO_2، Fe_2O_3 و α-Fe_2O_3/ TiO_2كإلكترونات مضادة. تم تحضير TiO_2, α-Fe_2O_3 النانوية وTiO_2/ α-Fe_2O_3 على ركائز (FTO) (القطب الأمامي) بينما يكون القطب الخلفي هو عبارة عن ركيزة من الكربون / الزجاج FTO. تم استخدام صبغتين طبيعيتين من الأصباغ صبغة الكراث الأخضر وصبغة الرمان الأحمر بينما يستخدم اليود / اليود (KI / I_2) كمحلول إلكتروليت. معدلات كفاءة الخلايا الشمسية هي (1.29,1.93,0.69) لـ TiO_2 , α-Fe_2O_3 و/TiO_2/ α-Fe_2O_3 صبغة الكراث الأخضر على التوالي. ومعدلات كفاءة الخلايا الشمسية (0.96,1.38,0.65) لـ TiO_2, α-Fe_2O_3 وTiO_2/ α-Fe_2O_3 / صبغة الرمان الحمراء على التوالي.

الكلمات المفتاحية: مركب نانوي ، حراري مائي ،خلايا شمسية صبغية.

1-INTRODUCTION

Nanomaterials are a fascinating group of materials that are in high demand for a wide range of uses in the real world.. A nanometer can be represented as a line of five silicon atoms or ten hydrogen atoms, each of which is one nanometer long. A substance is referred to as a nanomaterial if one of its dimensions is between 1 and 100 nm in size. It is challenging to determine the exact timeline of human use of nanoscale objects. [1]. The use of nanomaterials, however, has a long history, and humans have inadvertently employed them for a variety of purposes for a very long time. Humans first used asbestos nanofibers to strengthen ceramic mixes about 4500 years ago[2]. Hematite has been used in photo-catalysis for water oxidation in photo-electrochemical cells designed for water splitting because it is inexpensive, easy to build, harmless, abundant, and stable.[3]. Hematite has the potential to increase its catalytic activity for additional redox reactions, a possibility that

has not yet been investigated. Research in this area may result in sensor applications that use this substance. The creation of sensors with very low detection limits for specific materials has been prompted by the desire for tools that enable early detection in groundwater, seas, rivers, or soils. contaminants is a field of study that is gaining more and more attention[4]. Numerous industries, including photocatalysis, agriculture, dye-sensitized solar cells and medicinal devices, use nano-TiO_2 photo semiconductors[5].The application of TiO_2 nanoparticles in agriculture, however, is still relatively new and needs more research. Agricultural researchers continue to be interested in the nano-TiO_2 photo semiconductor due to its advantageous physical and chemical characteristics, low price, availability, and excellent stability[6]. As a result, nano-TiO_2 photo semiconductors offer a wide range of potential applications in agriculture, such as pesticide breakdown, plant protection, and residue detection. TiO_2 nanoparticles do have a drawback, though, in that their high band gap of about 3.2 ev makes them predominantly active in the presence of UV light[7]. Nanomaterials are at the very core of DSSC since current research into the utilization of natural ingredients in the manufacture of solar cells has been driven by the demand for a greener and more ecologically friendly energy generation[8]. Figure(1)shows the working principle of dyestuff solar cells. The central component of the system is an intermediate sheet of semiconductor oxide in contact with either an organic hole conductor or a redox electrolyte[9]. The surface of the nanocrystal layer has a monolayer of the dye sensitizer connected to it. The photon-absorbing dye sensitizer will work (light) under sunlight irradiation, and the photon's energy is sufficient to excite an electron from the dye. The HOMO level of the dye molecule is converted to LUMO and undergoes photocatalysis at the interface of the dye and TiO_2, due to the presence of an electron in TiO_2 and the presence of a hole in the oxidizing dye molecule, charge separation is achieved. Electron-adsorbing dye molecules enter the conduction band of anatase phase TiO_2 nanoparticles of the dye's LUMO level[10].

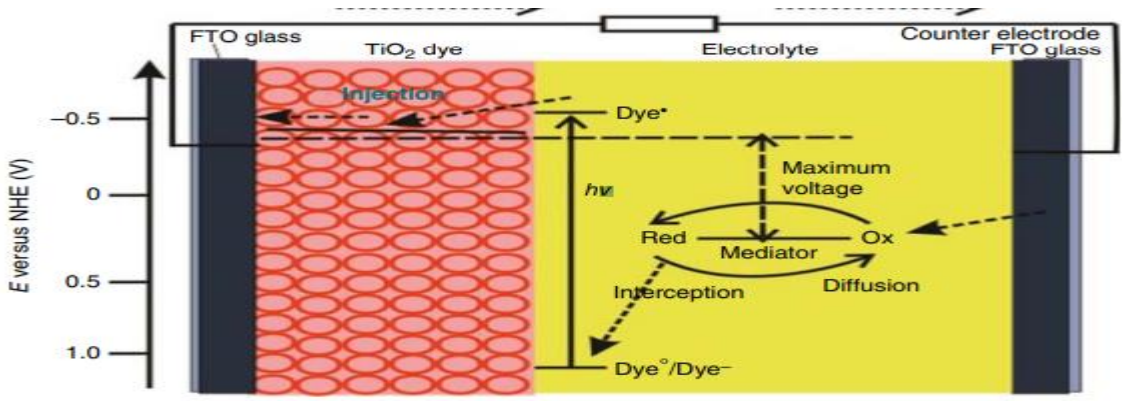

Figure 1. Diagram showing the DSSCs' operating system [9].

2-EXPERIMENTAL PART

2-1-Synthesis of α-Fe_2O_3 Nanoparticles and α-Fe_2O_3 /TiO_2 Nanocomposite

TiO_2, α-Fe_2O_3, and α-Fe_2O_3 /TiO_2 nanoparticles were prepared by the hydrothermal method. TiO_2 NPs were prepared by adding 1 mL of TTIP (Ti $(OC_3H_7)_4$ first and stirring for 30 min after mixing 25 mL of distilled water (DIW) with 25 mL of HCl 11.6 M. Then 30 mL of the prepared solution is transferred to a 70 mL sterile Teflon-lined stainless steel which for three hours at 140 C in an oven. TiO_2 yields a white precipitate. The final product is annealed at 400 C for three hours to improve crystallization after being centrifuged three times with distilled water and ethanol before drying at 90 C for three minutes. [11]. Fe_2O_3 NPs were prepared by dissolving 4.052 g of iron (III) chloride hexahydrate $FeCl_3$, $6H_2O$ in 100 mL of deoxygenated distilled water for 30 min at 80 C° with magnetic stirring. To maintain the pH at 11, 50 mL of sodium hydroxide (0.6 mol/L). The solution was placed in a Teflon-lined stainless steel autoclave for 12 h at 160 C°. The resulting precipitate was separated by centrifugation, then washed several times with distilled water and ethanol and calcined at 450 C° for four hours [12]. The hydrothermal method was used to synthesize α-Fe_2O_3/TiO_2 nanocomposites 3.376 g of $FeCl_3.6H_2O$ and 1.0 g TiO_2 nanofibers in equal proportions (1:1) that were dissolved in 80 ml deionized water and 0.2 mL ammonia. in the solution. The final product was put into a Teflon-lined autoclave with a 40 mL capacity. The autoclave was sealed and heated for four hours at 95 C before being cooled to room temperature Ethanol and deionized water was used for collection and washing.The products were annealed in 500C° (2 h) oven after drying at 60 C° for 24 h [13].

2-2-Material and Methods.

The properties of the prepared compounds are examined utilizing transmission electron microscopy (TEM), field emission scanning electron microscopy (FE-SEM), and X-rays diffraction. All chemicals in this work were obtained from the Merck business and utilized without additional purification such as. NaOH, TTIP Ti (OC_3H_7) and $FeCl_3.6H_2O$. The solar cell's efficiency was determined using a Programmable Keithley electrometer (2400) with the relation

$$FF=J_{MAX} *V_{MAX}/J_{SC}* V_{OC} \quad (1)$$

where J_{MAX} is the maximum current, V_{MAX} is the maximum voltage, J_{SC} is the short-circuit current and V_{OC} is the open-circuit voltage. [14].

3-RESULTS AND DISCUSSIONS

3-1-X-rays diffraction analysis

Figure 3. shows the result of TiO_2 NPs prepared by hydrothermal pH=9 at $400C^0$ the crystal structure is a tetragonal structure with space group (I41/amd) and lattice parameters were a = b = 3.776 Å, c = 9.486 Å to the miller indices (hkl) values (101) (004) (200) (105) (211) (204) (220) and (215), respectively corresponding to (JCPDS card no. 01-073-1764) [16]. Nonetheless, no additional peaks were identified that could have been caused by the contaminant. The nano-sized TiO_2 has a very high crystallinity, as evidenced by the sharp peaks [17]. Figure (4) depicts the ilmenite ore's XRD patterns and the α -Fe_2O_3/TiO_2 mixed oxides that resulted from calcining it at 500 C for two hours All diffraction peaks in the XRD pattern of ilmenite ore may be attributed to the Ilmenite α-Fe_2O_3 /TiO_2 phase (JCPDS card No. 98-010-4235). The XRD pattern shows that α-Fe_2O_3 /TiO_2 was transformed to (α-Fe2O_3 /TiO_2) mixed oxides after sintering at 500 C^0 for 2 hours in air condition and then proceeding to the ball mill operation. The XRD pattern was used to assign diffraction peaks to the TiO_2 rutile (JCPDS card number 98-006-2553) and α -Fe_2O_3 (hematite, JCPDS card number 98-005-3677) phase of the produced α-Fe_2O_3 /TiO_2 nanocomposite [18].

The following Scherrer's equation[19] was used to compute the crystalline size (D):

$$D\ (nm) = k.\lambda / \beta\cos\theta \qquad (2)$$

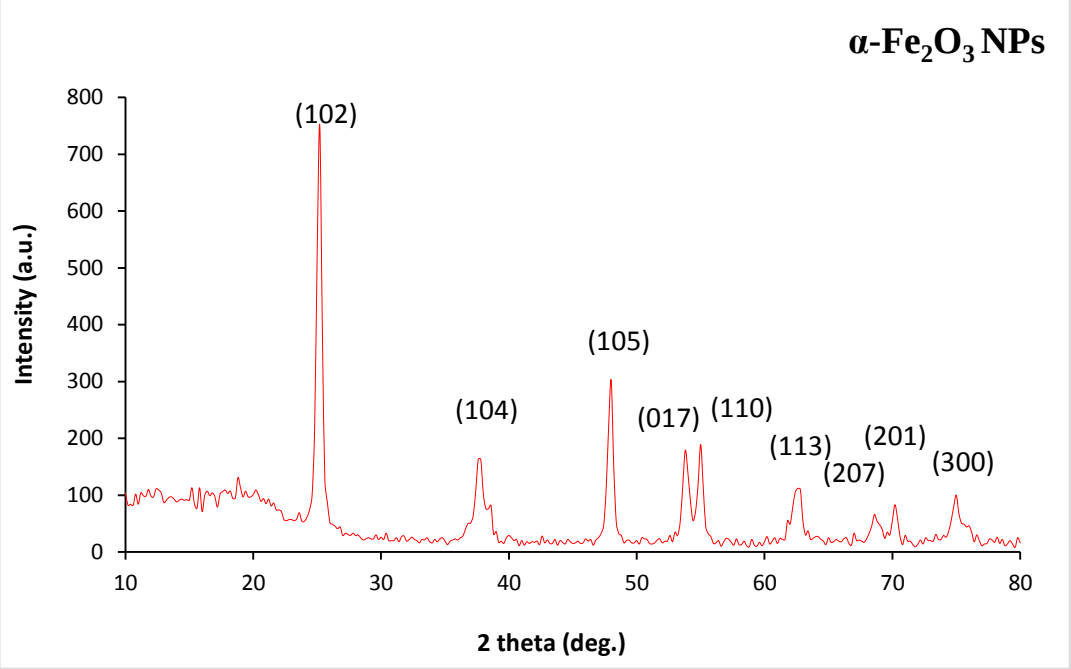

Figure 2. XRD patterns of α-Fe_2O_3 NPs prepared by hydrothermal method.

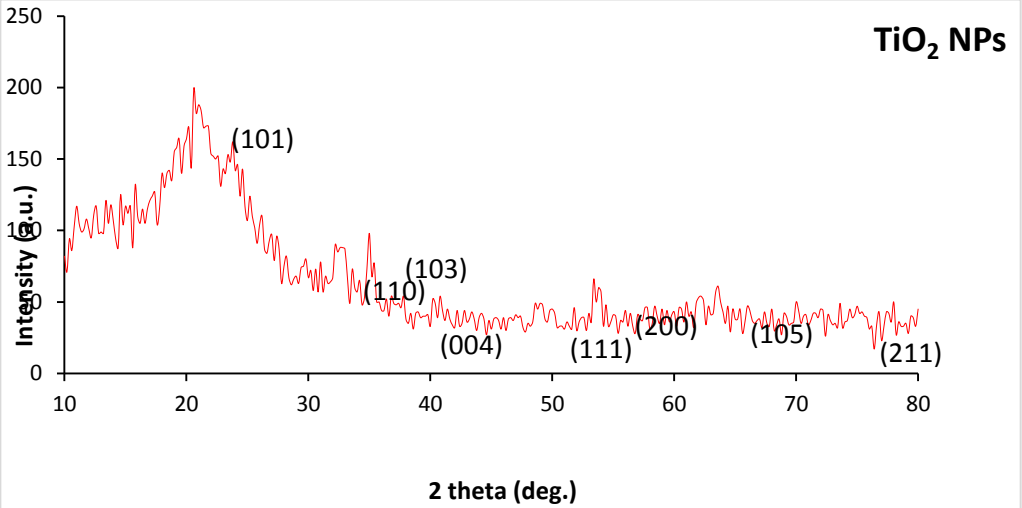

Figure 3. XRD patterns of TiO_2 NPs prepared by hydrothermal method.

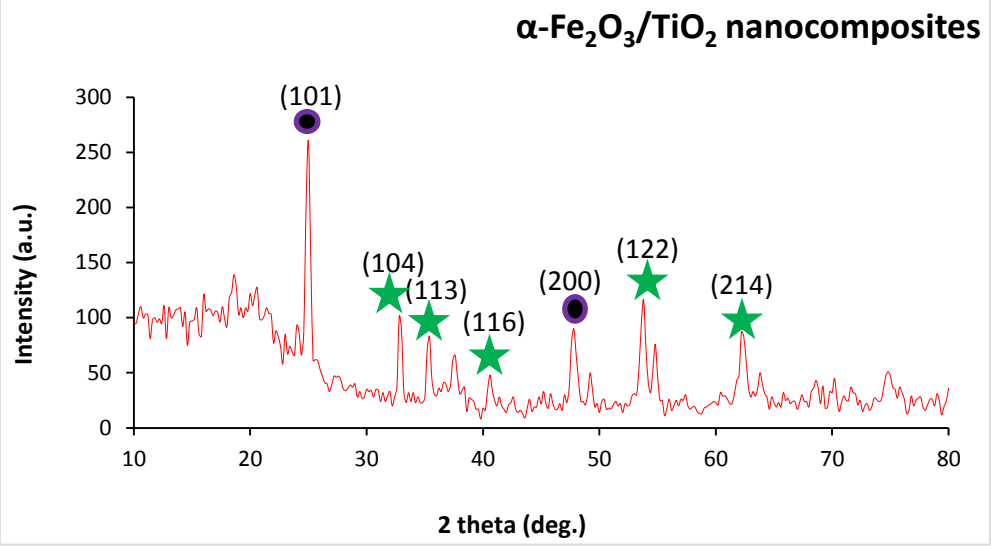

Figure 4. XRD patterns of α-Fe_2O_3/ TiO_2 nanocomposite at 400 C^O for 3 h.

3-2-FESEM Analysis of TiO_2, α-Fe_2O_3 NPs and α-Fe_2O_3 /TiO_2 Nanocomposites

Particle size and shape (40.69 to 60.67) nm and spherical structure of α-Fe2O3 NPs at 400 C^o for 3h at pH=10 by hydrothermal method, as shown in Figure. 5(A-D) [20]. Figure 6(A-D) shows the FE-SEM images of the TiO_2 nanoparticles (NPs) prepared by the Hydrothermal method at pH 8. It is clear that different morphology in a material, and particles. In figure 6(A-D), zones of TiO_2 where the bright points can be attributed to both free Ti and O_2 particles. The particle size was about (33.71 to 33.95) nm with nanoparticles [21] The shape of the α-Fe_2O_3/TiO_2 nanocomposite was studied using FESEM images Figure 7(A-D) revealing that the nanoparticles of α-Fe_2O_3 /TiO_2 nanocomposite were indeed formed. As seen in FESEM photos, the α-Fe_2O_3/TiO_2 nanocomposite is synthesized in an aggregated form. The particle size and shape are (39 to 43) nm and the spherical-like structure of α-Fe_2O_3 /TiO_2 nanocomposite at 400 C^0 for 2h at pH=10 by the hydrothermal method, as shown in figure 8 (A-D).

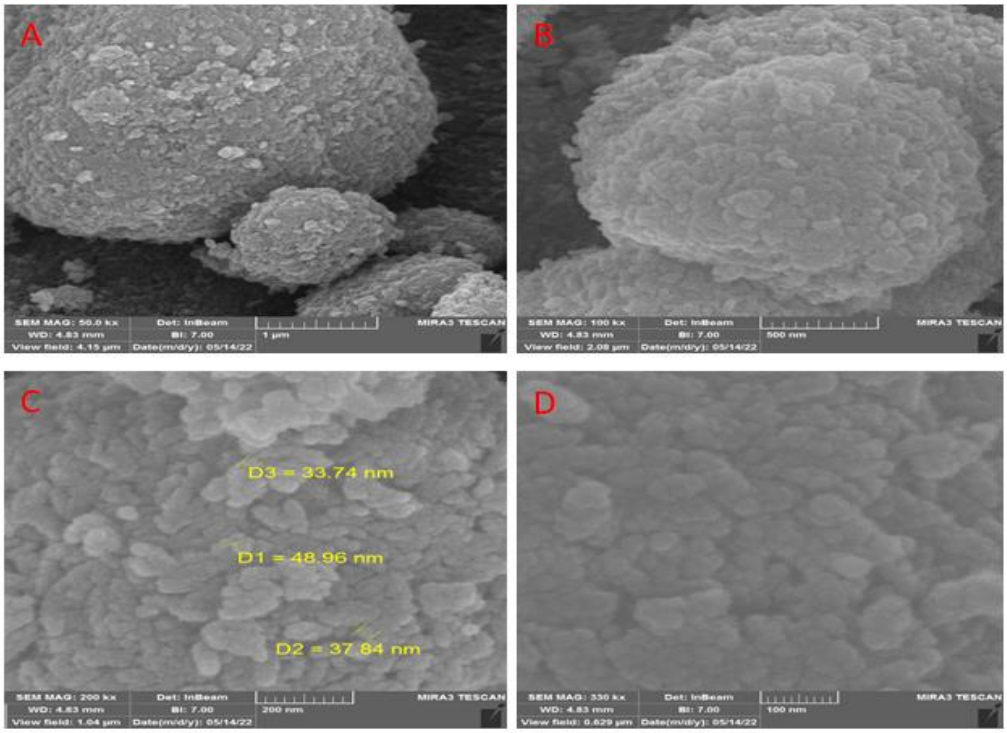

Figure 5. FE-SEM images of α-Fe_2O_3 NPs prepared by hydrothermal method at 400 C^0 for 3h at pH=10.

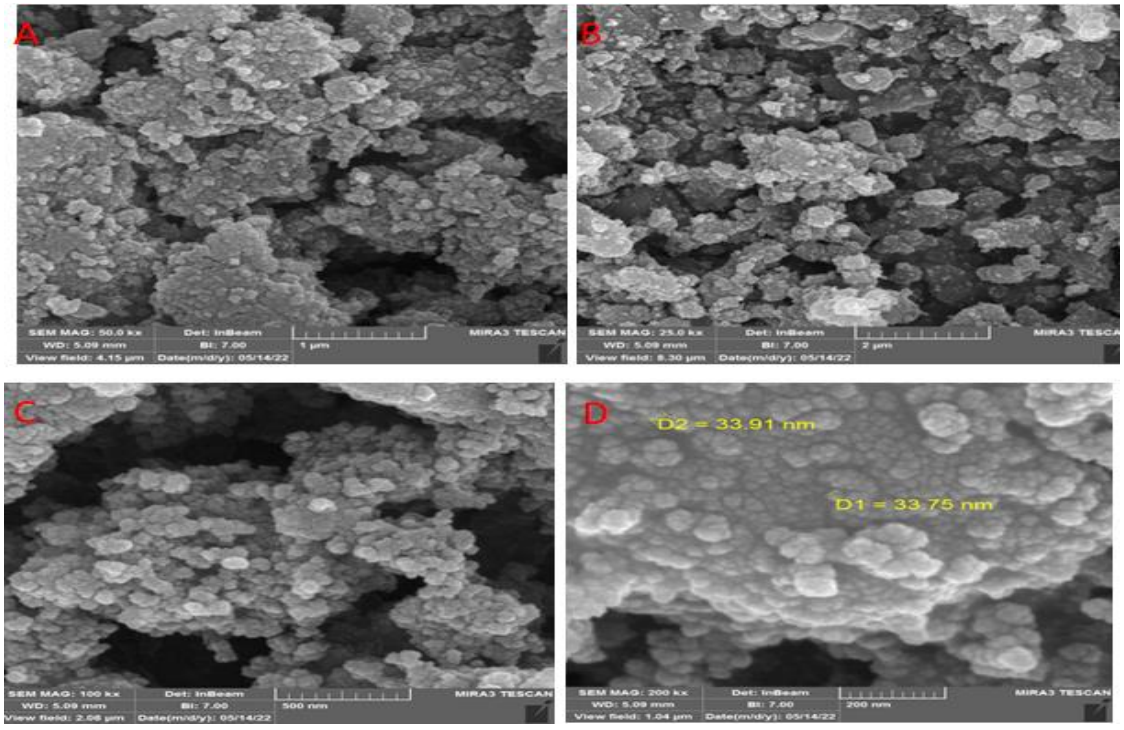

Figure 6. FE-SEM images of TiO_2 NPs prepared by hydrothermal method at 400 C^0 for 2h at pH=8.

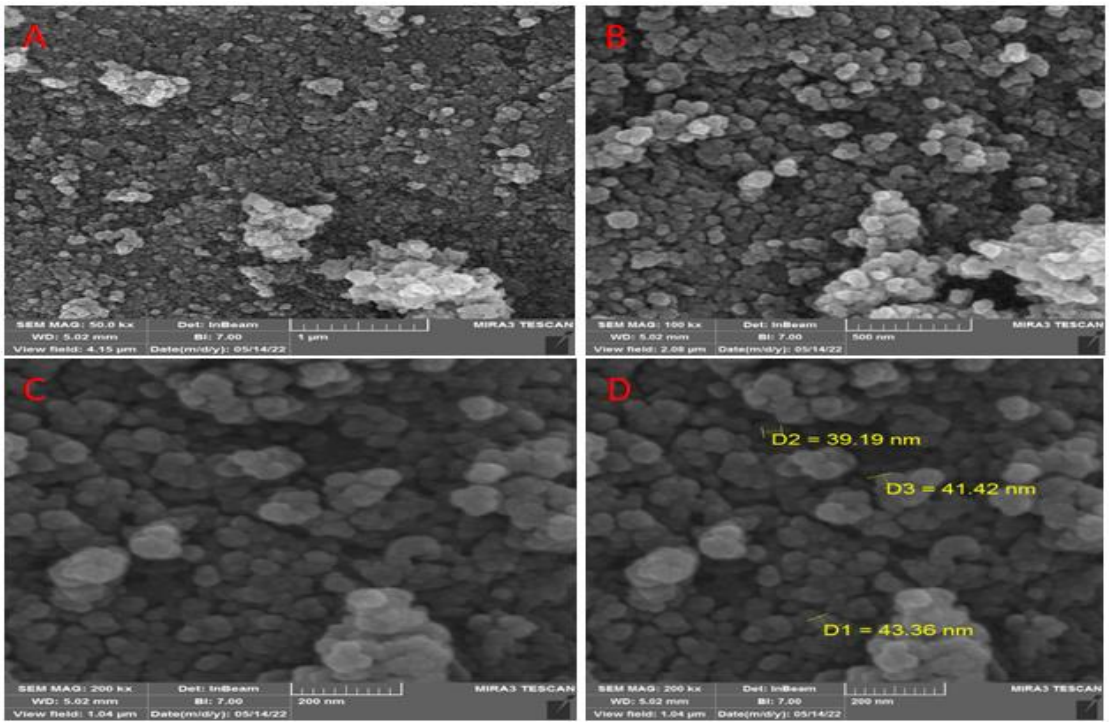

Figure7 .FE-SEM images of α-Fe_2O_3 / TiO_2 nanocomposite prepared by hydrothermal method at 400 C^0 for 3h.

3-3-TEM Analysis, α-Fe_2O_3 and TiO_2/ α-Fe_2O_3 Nanocomposites

Utilizing transmission electron microscopy, the morphology and typical grain size are examined. of pure α-Fe_2O_3 NPs, as shown in Figure 8 (A-D). The formation and growth of NPs provide the basis for this trend. NPs with small diameters can be developed thanks to a longer reaction time. There is some agreement between the size of the produced IONPs and the size described in the literature on solvent-less synthesis of IONPs by the hydrothermal technique. Changes in PH cause a decrease in the size of α-Fe_2O_3 NPs, from 15 to 20 nm with Nanorod nanoparticles. In this case, the longer the heating period, the smaller the NPs will be [22]. TEM images of Titanium oxide nanoparticles TiO_2 NPs prepared using the hydrothermal method at 400 C^o for 2h at pH=8, as in Figure 9(A-D), where the microscopic images confirm the formation of hexagonal nanoparticles since the fission process took place in a free medium without any capping factor, some particles were overlapping among themselves, as it was noted that some spherical nanoparticles appear large due to the phenomenon of agglomeration. The average grain size of TiO_2

nanoparticles was (23 to 49 nm) [23]. Both samples' TEM images are shown in Figure 10(A, B). Small agglomerated particles of varying sizes and shapes (cubic, and spherical) were present in both samples, possibly as a result of coalescence [24]State that the sintering temperature and neighboring particles in contact that can coalesce into a huge grain size particle determine the particle size distribution in agglomerates. For (1:1) α-Fe_2O_3 /TiO_2, The typical grain size was determined to be between (15 and 45) nm, demonstrating that adding more TiO_2 resulted in smaller particles overall [25].

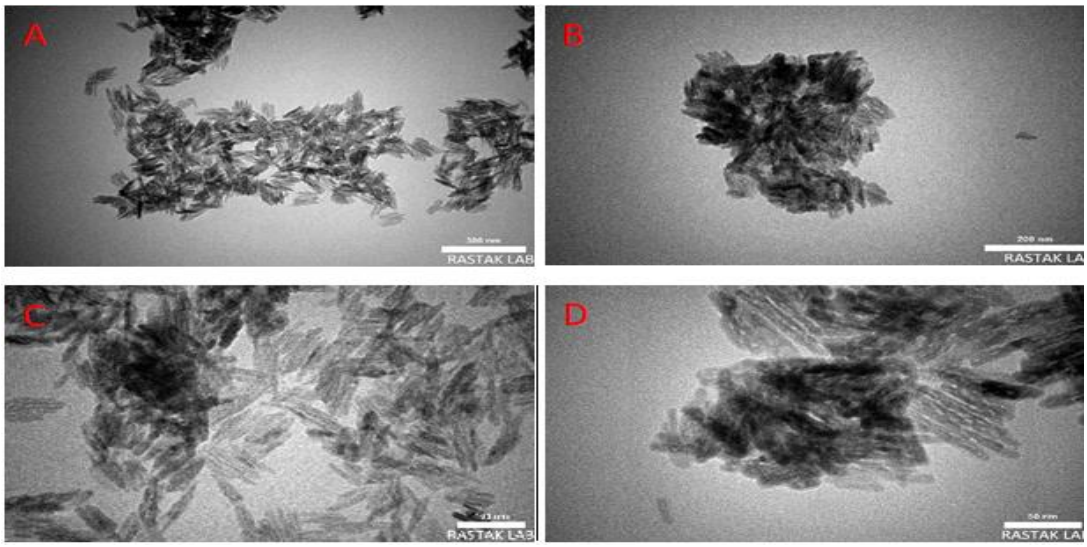

Figure 8. TEM images of α-Fe_2O_3 NPs prepared by hydrothermal .

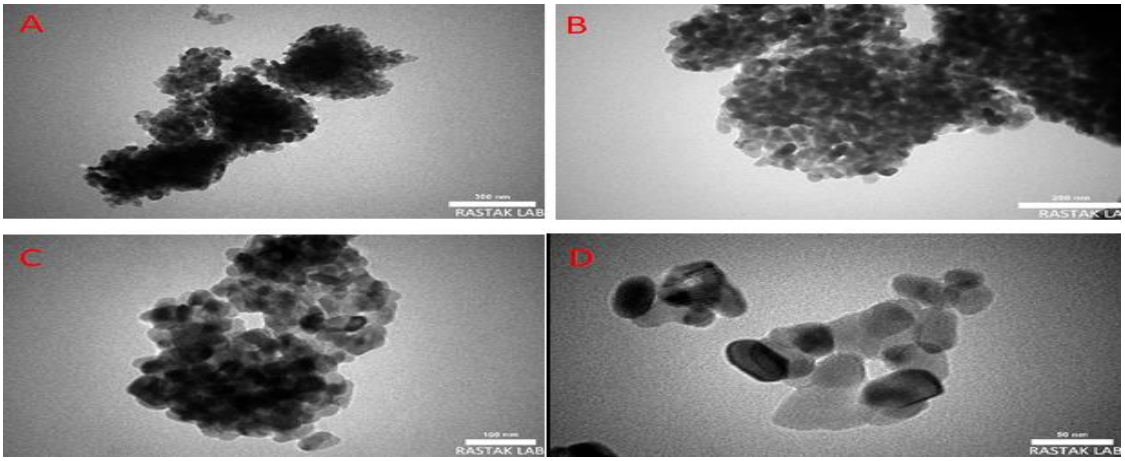

Figure 9. TEM images of TiO_2 NPs prepared by hydrothermal method.

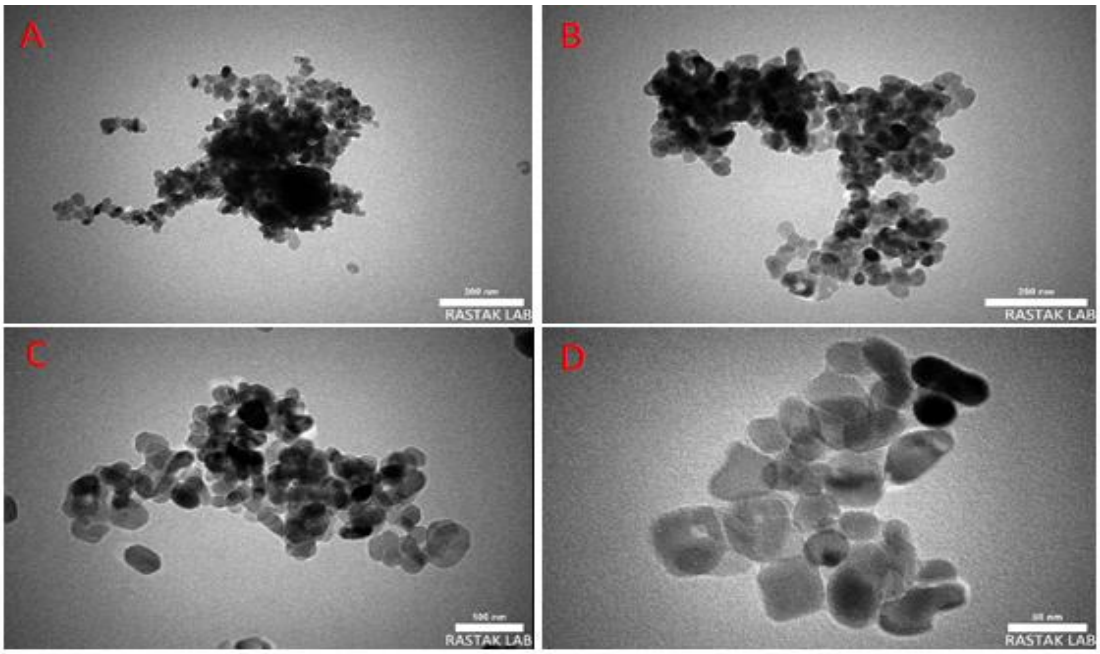

Figure10. TEM images of α-Fe_2O_3/TiO_2 nanocomposite prepared by hydrothermal method.

3-4-Optical Properties

The absorption spectra and energy band gap α-Fe_2O_3, TiO_2 nanoparticles and α-Fe_2O_3/TiO_2 nanocomposites are shown in Figures. (11-14) respectively and Table 1.

Table 1. shows the energy band gap of α -Fe_2O_3, TiO_2 and α-Fe_2O_3 /TiO_2.

TiO_2	3.0 ev
α-Fe_2O_3	1.6ev
α-Fe_2O_3 /TiO_2	2.7 ev

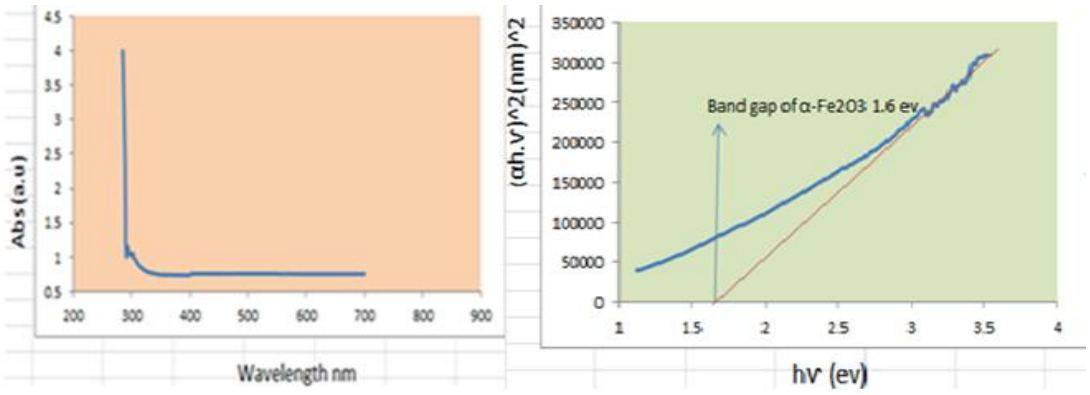

Figure13. The optical band gap and absorbance spectrum of α-Fe_2O_3 nanoparticles.

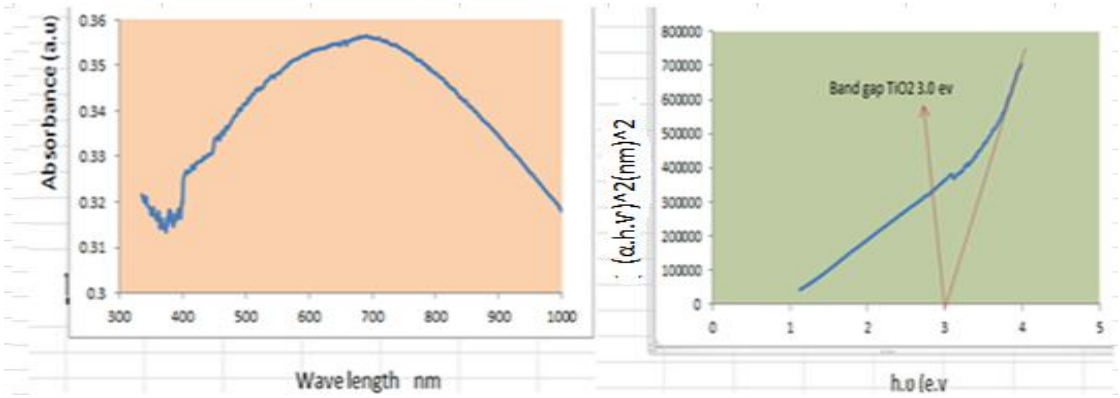

Figure.12. The optical band gap and absorbance spectrum of TiO_2 nanoparticles.

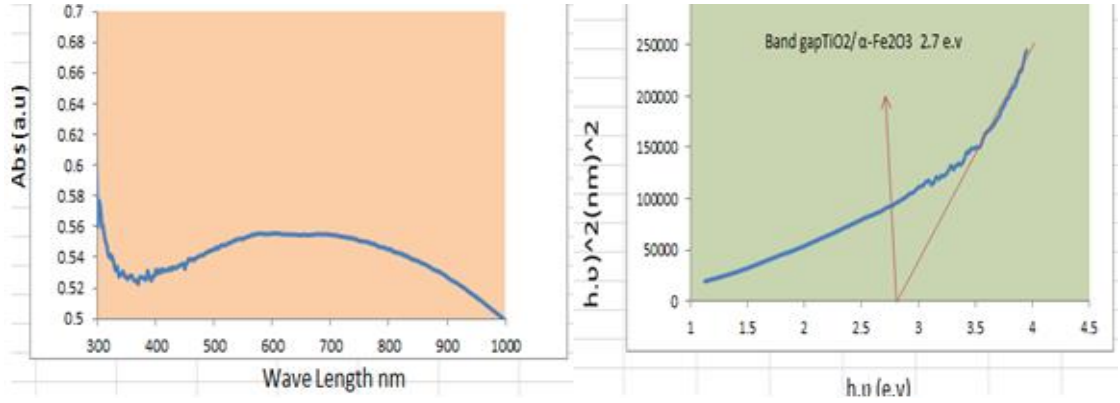

Figure13. The optical band gap and absorbance spectrum of TiO_2/ α-Fe_2O_3 nanoparticles.

4-The Applications of α-Fe_2O_3, TiO_2 nanoparticles and α-Fe_2O_3/TiO_2 nanocomposites in Solar Cells.

4-1-Fabrication of Dye-Sensitized Solar Cells.

DSSCs are fabricated using α-Fe_2O_3, TiO_2 nanoparticles and α-Fe_2O_3 /TiO_2 nanocomposites as photoelectrode and two natural dyes, red pomegranate dye and green leek dye were used as an absorbent medium. Figure 14(A,B, C) shows the I-V characteristics of DSSCs prepared based on α-Fe_2O_3 , TiO_2 nanoparticles and α-Fe_2O_3 TiO_2 nanocomposites / green leek dye have given V_{OC}, I_{SC} and efficiency (η%) are shown in a Table(2).

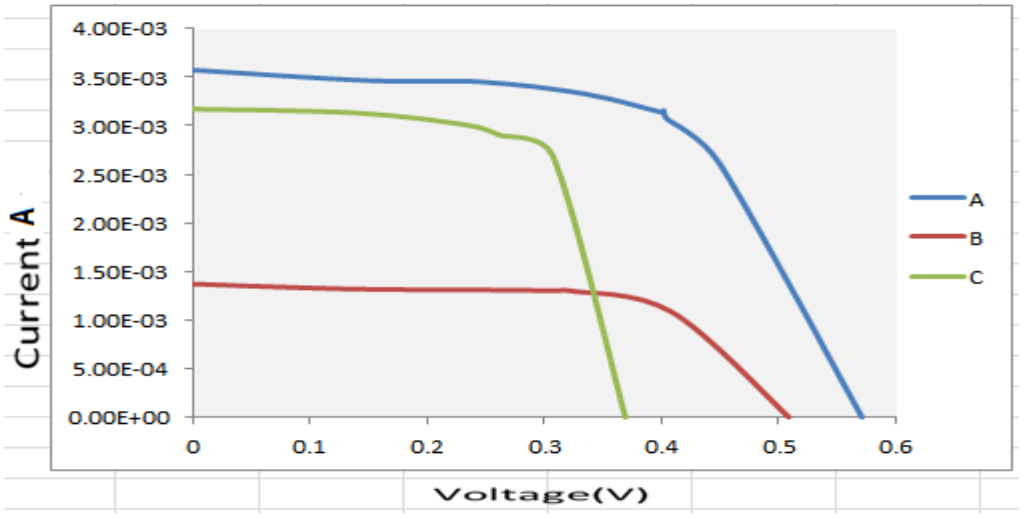

Figure14.I-V characteristics of prepared DSSCs (A) α-Fe_2O_3 , (B) TiO_2 and(C) α-Fe_2O_3/TiO_2/ green leek dye

Table2.Photoelectrochemical parameters of the DSSCs, A=0.25cm^2 under intensity light 28.2 Mw/cm^2 using/ green leek dye.

Catalyst/ gree n .leek dye	I_{SC} mA	V_{OC} (V)	I_{max} Ma	V_{max} (V)	P_{max}	FF%	%η
α-Fe_2O_3	3.58	0.71	3.07	0.404	1.24	60	1.93
TiO_2	1.31	0.507	1.08	0.408	0.440	66	0.69
α-Fe_2O_3 /TiO_2	3.17	0.368	2.69	0.307	0.755	69	1.29

Figure15(A, B, C) show the I-V characteristics of DSSCs prepared depending on α-Fe_2O_3, TiO_2 nanoparticles and TiO_2/ α-Fe_2O_3 nanocomposites/red pomegranate dye has given V_{OC}, I_{SC} and efficiency (η%) are shown in a Table(3).

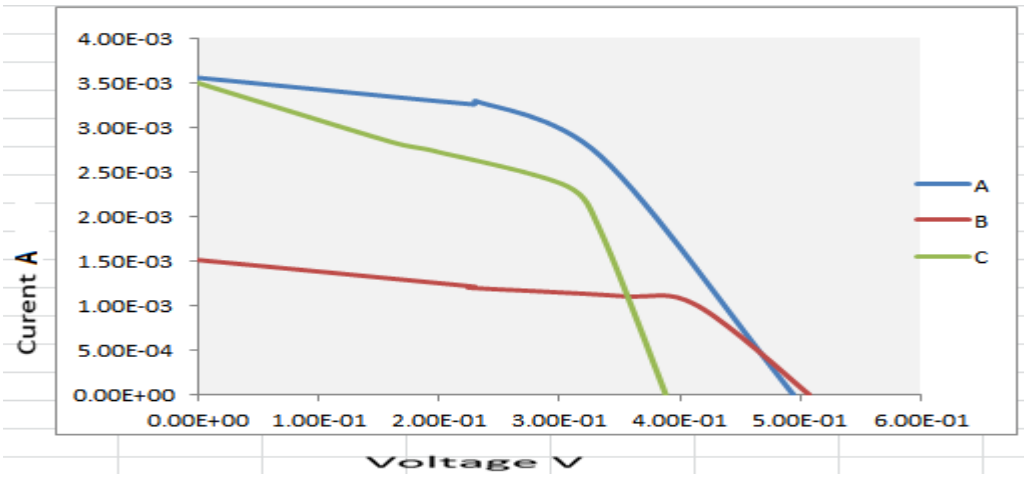

Figure15.I-V characteristics of prepared DSSCs, (A) α-Fe_2O_3 , (B) TiO_2 and(C) α-Fe_2O_3 /TiO_2/ red pomegranate dye

Table.3. Photo electrochemical parameters of the DSSCs, A=0.25cm^2 under intensity light28.2 M w/cm^2 using red pomegranate dye.

Catalyst// red pomegranate .dye	I_{SC} mA	V_{OC} (V)	I_{max} mA	V_{max} (V)	P_{max}	FF%	**η%**
α-Fe_2O_3	3.53	0.494	2.68	0.334	0.985	50	1.38
TiO_2	1.51	0.507	1.00	0.414	0.414	54	0.65
α-Fe_2O_3 /TiO_2	3.51	0.388	1.83	0.334	0.611	45	0.96

The results showed that the efficiency of DSSC made based on α-Fe_2O_3 with green leek dye and red pomegranate dye is higher than that of TiO_2 NPs and TiO_2/ α-Fe_2O_3 nanocomposites. there are many reasons. First, it has a low energy gap (1.6 ev) in α-Fe_2O_3. As the energy gaps decrease the efficiency increases. This is because lower energy gaps enable electrons with greater solar energy efficiency and lower excitation energy to become free electrons in a conduction band. [26],[27]. Second, the surface area of α-Fe_2O_3 is 74.604m^2/g and is higher than of TiO_2 NPs and TiO_2/ α-Fe_2O_3 nanocomposites, Which indicates an increase in dye adsorption on the surface of α-Fe_2O_3 which may lead to an increase in the efficiency of the fabricated DSSC[28]. In addition, the current yield of DSSCs with natural dye (pomegranate red dye) is lower than that of DSSCs made using leek green dye due to the energy gap of leek green dye (1.83ev). Less than red pomegranate tincture (2.34ev). Thus they have low efficiency compared to that (2. 43ev) which is very near to the conduction band thus electrons easily become free and thus have higher efficiency[29]. The second reason is that the leek pigment is the pigment chlorophyll, which has an excess of electrons and can provide these electrons to the cell better than the anthocyanin pigment found in red pomegranate.[30]. Moreover, the lower value obtained from the manufactured DSSCs is also due to the low density (28.2 mW/cm^2) of the light source used.

Conclusions:-

α-Fe_2O_3, TiO2 and TiO_2/α-Fe_2O_3 nanoparticles are prepared by a quick and secure hydrothermal technique. Semiconductor deposition on FTO glass by doctor blade gives a better homogeneous surface than dropping and evaporation of semiconductor solution suspended on FTO Similarly, deposited graphite gave a homogeneous and more stable surface than using candle flame which is quickly removed from a glass surface. Several techniques have been used to describe the products equipped with Transmission electron microscopy (TEM), X-ray diffraction, and field emission scanning electron microscopy (FE-SEM). It is noted from the previous data that the dye has a very important role in improving the efficiency of the solar cell, as the results showed that the cells made from green leek dye produce much higher efficiency than cells prepared from red pomegranate dye in all cases. The results also showed that the cells prepared from α-Fe_2O_3 NPs with better efficiency than TiO_2 and α-Fe_2O_3/TiO_2.

REFERENCES

1. Muhajir, M., P. Puspitasari, and J.A. Razak, *Synthesis and applications of Hematite α-Fe2O3: A Review.* J. Mech. Eng. Sci. Technol, 2019. **3**(2): p. 51-58.
2. Baig, N., I. Kammakakam, and W. Falath, *Nanomaterials: A review of synthesis methods, properties ،recent progress, and challenges.* Materials Advances, 2021. **2**(6): p. 1821-1871.
3. Qin, Q., D. Olimov, and L. Yin, *Semiconductor-Type Gas Sensors Based on γ-Fe2O3 Nanoparticles and Its Derivatives in Conjunction with SnO2 and Graphene.* Chemosensors, 2022 :(7)10 .p. 267.
4. Rahman, M.M., et al., *Semiconductor α-Fe2O3 Hematite Fabricated Electrode for Sensitive Detection of Phenolic Pollutants.* ChemistrySelect, 2018. **3**(43): p. 12169-12174.
5. Wang, Y., et al., *The Application of Nano-TiO(2) Photo Semiconductors in Agriculture.* Nanoscale Res Lett, 2016. **11**(1): p. 529.
6. Rodríguez-González, V., C. Terashima, and A. Fujishima, *Applications of photocatalytic titanium dioxide-based nanomaterials in sustainable agriculture.* Journal of Photochemistry and Photobiology C: Photochemistry Reviews, 2019. **40**: p. 49-67.
7. Chouhan, L. and S. Srivastava, *Observation of room temperature d0 ferromagnetism, band-gap widening, zero dielectric loss and conductivity enhancement in Mg doped TiO2 (rutile+ anatase) compounds for spintronics applications.* Journal of Solid State Chemistry, 2022. **307**: p. 122828.
8. Jiao, Y., et al., *Dye sensitized solar cells principles and new design.* Solar Cells-Dye-Sensitized Devices, 2011. **1**(1.(
9. Karthick, S., et al., *Dye-sensitized solar cells: history, components, configuration, and working principle.* Interfacial Engineering in Functional Materials for Dye-Sensitized Solar Cells, 2019: p. 1-16.
10. Najm, A.S., et al., *N719 dye as a sensitizer for dye-sensitized solar cells (DSSCs): A review of its functions and certain rudimentary principles.* Environmental Progress & Sustainable Energy, 2022: p. e13955.

11. Spiridonova, J., et al., *Effect of the titanium isopropoxide: acetylacetone molar ratio on the photocatalytic activity of TiO2 thin films.* Molecules, 2019. **24**(23): p. 4326.
12. Li, Z., et al., *Facile synthesis of α-Fe2O3 micro-ellipsoids by surfactant-free hydrothermal method for sub-ppm level H2S detection.* Materials & Design, 2016. **110**: p. 532-539.
13. Lou, Z., et al., *Branch-like hierarchical heterostructure (α-Fe2O3 /TiO2): a novel sensing material for trimethylamine gas sensor.* ACS applied materials & interfaces, 2013. **5**(23): p. 12310-12316.
14 Aljumaili, M., A. Abdalkafor, and M. Taha, *Analysis of the Hard and Soft Shading Impact on Photovoltaic Module Performance Using Solar Module Tester.* International Journal of Power Electronics and Drive Systems, 2019. **10**.
15. Padil, V.V.T. and M. Černík, *Green synthesis of copper oxide nanoparticles using gum karaya as a biotemplate and their antibacterial application.* International journal of nanomedicine, 2013. **8**: p. 889.
16. Singh, A., et al., *Structural, morphological, optical and photocatalytic properties of green synthesized TiO2 NPs.* Current Research in Green and Sustainable Chemistry ׃3 .2020 ،p. 100033.
17. Reveendran, R. and M.A. Khadar. *Synthesis, characterization and electrical properties of α-Fe2O3 /CuO nanocomposites*. in *AIP Conference Proceedings*. 2019. AIP Publishing LLC.
18. Saleh, T.A., *Simultaneous adsorptive desulfurization of diesel fuel over bimetallic nanoparticles loaded on activated carbon.* Journal of Cleaner Production, 2018. **172**: p. 2123-2132.
19. Rabiee, N., et al., *Biosynthesis of copper oxide nanoparticles with potential biomedical applications.* International Journal of Nanomedicine, 2020. **15**: p. 3983.
20. Riaz, N., et al. *Visible light photodegradation of azo dye by Cu/TiO2*. in *Advanced Materials Research*. 2014. Trans Tech Publ.
21. Gao, Y., et al., *Construction of Fe2O3@ CuO heterojunction nanotubes for enhanced oxygen evolution reaction.* ACS Applied Energy Materials, 2019. **3**(1): p. 666-674.
22. Pan, L., J. Tang, and F. Wang, *Facile synthesis of nanoscaled α-Fe2O3 , CuO and CuO/Fe2O3 hybrid oxides and their electrocatalytic and photocatalytic properties.* Open Chemistry, 2013. **11**(5): p. 763-773.
23. Liu, Z. and C. Zhou, *Improved photocatalytic activity of nano CuO-incorporated TiO2 granules prepared by spray drying.* Progress in Natural Science: Materials International, 2015. **25**(4): p. 334-341.
24. Da Rosa, E.L.S ،.*Kinetic effects of TiO2 fine particles and nanoparticles aggregates on the nanomechanical properties of human neutrophils assessed by force spectroscopy.* BMC biophysics, 2013. **6**(1): p. 1-10.
25. Hassan, D.F. and M.B. Mahmood, *Using of iron oxide nanoparticles and application in the removing of heavy metals from sewage water.* Iraqi Journal of Science, 2019. **60**(4): p. 732-738.
26. Elhouri, S.A., *The Value of Efficiency and Energy Gap for Different Dye Solar Cells.* Global Journal of Engineering Science and Researches, 2018. **5**(8): p. 115-121.
27. Contreras, M.A., et al. *Improved energy conversion efficiency in wide bandgap Cu (In, Ga) Se 2 solar cells*. in *2011 37th IEEE Photovoltaic Specialists Conference*. 2011. IEEE.
28. Son, Y.J., et al., *Influence of TiO2 particle size on dye-sensitized solar cells employing an organic sensitizer and a cobalt (III/II) redox electrolyte.* The Journal of Physical Chemistry C, 2018. **122**(13): p. 7051-7060.
29. Bokov, D., et al., *Nanomaterial by sol-gel method: synthesis and application.* Advances in Materials Science and Engineering, 2021. **2021**.
30. Syafinar, R., et al., *Chlorophyll pigments as nature based dye for dye-sensitized solar cell (DSSC).* Energy Procedia, 2015. **79**: p. 896-902.